

From Linear Probing to **J**oint-**W**eighted **T**oken **H**ierarchy: A Foundation Model Bridging Global and Cellular Representations in Biomarker Detection

Jingsong Liu^{1,3,4*}, Han Li^{2,3}, Nassir Navab^{2,3},
Peter J. Schüffler^{1,3,4*}

^{1*}Institute of Pathology, TUM School of Medicine and Health,
Munich, Germany.

²Computer Aided Medical Procedures (CAMP), TU Munich,
Munich, Germany.

³Munich Center for Machine Learning (MCML), Munich, Germany.

⁴Munich Data Science Institute (MDSI), Munich, Germany.

*Corresponding author(s). E-mail(s): jingsong.liu@tum.de;
peter.schueffler@tum.de;

Abstract

AI-based biomarkers can infer molecular features directly from hematoxylin & eosin (**H&E**) slides, yet most pathology foundation models (PFMs) rely on global patch-level embeddings and overlook cell-level morphology. We present a PFM model, **JWTH** (**J**oint-**W**eighted **T**oken **H**ierarchy), which integrates large-scale self-supervised pretraining with cell-centric post-tuning and attention pooling to fuse local and global tokens. Across four tasks involving four biomarkers and eight cohorts, **JWTH** achieves up to **8.3%** higher balanced accuracy and **1.2%** average improvement over prior PFMs, advancing interpretable and robust AI-based biomarker detection in digital pathology.

Keywords: Pathology Foundation Model, Biomarker detection, Self-supervised Learning

1 Introduction

Computational pathology has emerged as a powerful paradigm for quantitative tissue analysis, bridging histopathology with modern artificial intelligence (AI). By leveraging whole slide images (WSIs) and deep learning (DL) techniques, computational pathology enables the extraction of morphological and molecular features directly from digitised slides [1–3]. These advances have transformed routine histology into a data-rich modality, offering new opportunities for biomarker discovery, cancer diagnosis, and treatment stratification [4, 5].

Among recent advances, pathology foundation models (PFMs) [6–8] trained on massive and diverse histopathology patches have shown strong potential for biomarker prediction directly from hematoxylin–eosin (H&E) stained slides. Following large-scale pretraining, these models can be readily adapted to biomarker prediction tasks, including MSI, HER2, and key oncogenic mutations [9–11]. Compared with traditional end-to-end convolutional architectures (e.g., ResNet variants), which typically require extensive annotated data and task-specific optimization [12], pretrained PFMs provide a scalable and label-efficient approach that generalizes across tumor types and cohorts, enabling robust biomarker inference even in data-limited low-resources settings.

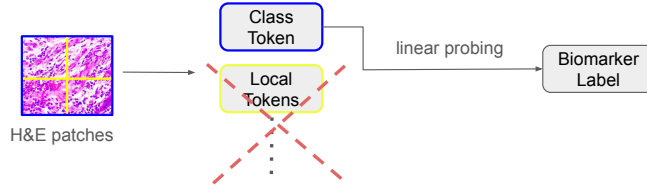
However, the existing methods often rely primarily on global patch-level embeddings, which capture broad tissue context but overlook fine-grained cell-level cues and the intricate spatial organization of the tumor microenvironment [13]. Such limitations may hinder the accurate quantification of molecular signals that manifest through subtle cellular morphology or inter-cell interactions. Capturing these local patterns is particularly critical when inferring biomarkers, where microarchitectural heterogeneity can serve as a key diagnostic determinant [14–16].

To overcome these challenges, recent research trends advocate for hierarchical representations that integrate both global and local features to enrich downstream predictions [17–19]. By combining patch- and cell-scale information, computational models can more faithfully reflect histological complexity, ultimately enhancing the interpretability and accuracy of biomarker prediction. However, this paradigm also exposes the *Achilles’ heel* of current PFMs—the effectiveness of their multi-level representations. Although PFMs encode abundant morphological information, their cell-level features often contain substantial noise due to sub-optimal pretraining objectives and insufficient cellular supervision [20, 21], which limits their ability to capture precise fine-grained diagnostic cues.

To this end, we propose a novel pathology foundation model, **JWTH**, tailored specifically for AI-based biomarker detection. Similar to existing PFMs, JWTH learns comprehensive global representations through large-scale pretraining on millions of patches spanning over 20 organs. To further enhance the precision of fine-grained representations, the model is post-tuned with a cell-centric regularization objective, reinforcing biologically meaningful cues such as nuclear morphology and tissue microarchitecture. By coupling these refined cellular descriptors with global contextual features via a multi-head attention fusion mechanism, JWTH achieves robust and interpretable biomarker prediction (Fig. 1).

Extensive experiments across six tasks covering four biomarkers and eight independent cohorts demonstrate the superior performance and generalization of JWTH.

(a) PFMs discard local cues for patches:



(b) **Our solution:**

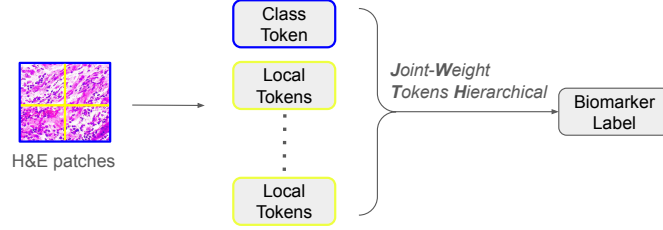


Fig. 1 (a) Existing pathology foundation model (PFM) pipelines typically rely on linear probing over the global class token, discarding fine-grained local cues from patch-level embeddings and thus losing critical cellular information. (b) Our proposed JWTH (Joint-Weight Token Hierarchy) integrates both class and local tokens through a multi-head attention mechanism, enabling the model to jointly reason over global tissue context and cell-level morphology for more accurate biomarker prediction.

The model consistently outperforms prior state-of-the-art PFMs, achieving up to 8.3% higher balanced accuracy in the most favorable case and an average improvement of 1.2% across all tasks (Fig. 2). Beyond performance gains, JWTH underscores the emerging potential of cell-aware foundation models as reliable AI-based biomarkers, bridging large-scale representation learning with clinically actionable precision oncology.

2 Method

2.1 Pathology Foundation Model

2.1.1 Data Preparation.

The training data comprise approximately 84 million patches extracted from 84,000 hematoxylin & eosin (H&E) stained whole-slide images (WSIs) scanned at $40\times$ magnification across more than ten tissue types at the Technical University of Munich Pathology Institute. Each WSI is first segmented using Otsu’s thresholding to isolate tissue regions, which are then subdivided into non-overlapping tiles of size 256×256 pixels.

2.1.2 Staining Augmentation.

A major challenge in computational pathology is domain shift, which arises from variations across pathology centers, including differences in staining protocols, scanner

settings, and digitization procedures [17]. To develop a general-purpose biomarker detection model, the foundation model (**FM**) must be robust to such staining shifts to ensure reliable deployment across different hospitals and laboratories. For this reason, we apply random staining augmentation [22] to image patches during self-supervised pretraining. Specifically, random perturbations are sampled from a Gaussian distribution and applied to the LAB and HSV color channels of the TUM pathology patches.

2.1.3 Large-Scale Pretraining.

Following [23], the large-scale training process consists of two stages: self-supervised pretraining and Gram-anchored post-training.

Pretraining stage. The model is trained using a combination of global and local loss objectives. Specifically, we employ an image-level objective L_{DINO} balanced with a patch-level latent reconstruction objective L_{iBOT} . Additionally, to prevent feature collapse [24] and encourage uniform feature dispersion, a Koleso regularization term is applied. The overall objective for the pretraining stage is given by:

$$L_{\text{pretraining}} = L_{\text{DINO}} + L_{\text{iBOT}} + L_{\text{Koleso}}. \quad (1)$$

Gram-Anchoring Post-Training. To enhance the model’s ability to encode fine-grained cellular information from **H&E** patches, it is necessary to stabilize and diversify the representations of local tokens. Previous PFMs [7, 8], due to large-scale pretraining, often exhibit inconsistency or collapse in fine-grained local token embeddings rather than progressive improvement during optimization [25]. To address this, we adopt Gram-anchoring [23] on a checkpoint obtained from the pretraining stage, introducing an additional term L_{Gram} into the loss function. The post-training objective is therefore formulated as:

$$L_{\text{posttraining}} = L_{\text{DINO}} + L_{\text{iBOT}} + L_{\text{Koleso}} + L_{\text{Gram}}. \quad (2)$$

This procedure encourages diversity among local token embeddings, resulting in more stable and informative cell-level representations.

2.2 Beyond Linear Probing

2.2.1 Problem Definition.

In a vision transformer (ViT)-based **PFM**, a histopathology image patch $\mathbf{I} \in \mathbb{R}^{H \times W \times 3}$ is divided into a grid of non-overlapping tokens of size $t \times t$. Each token is linearly projected into a feature embedding and appended with a learnable class token \mathbf{z}_{cls} representing global information. The resulting input sequence is defined as:

$$\mathbf{Z}_0 = [\mathbf{z}_{\text{cls}}; \mathbf{E}(\mathbf{x}_1), \mathbf{E}(\mathbf{x}_2), \dots, \mathbf{E}(\mathbf{x}_N)] + \mathbf{E}_{\text{pos}}, \quad (3)$$

where $\mathbf{E}(\cdot)$ is the patch embedding function, \mathbf{E}_{pos} denotes positional encodings, and $N = (H/t) \times (W/t)$ is the number of patch tokens. After L transformer layers, the final hidden representation $\mathbf{Z}_L = [\mathbf{z}_{\text{cls}}^L, \mathbf{z}_1^L, \dots, \mathbf{z}_N^L]$ is obtained.

2.2.2 Linear Probing.

Existing PFM-based pipelines typically employ **linear probing** to evaluate the pre-trained representations, as fine-tuning large transformer encoders is computationally expensive and often unstable [26]. Therefore, the pretrained encoder is kept frozen, and a lightweight linear classifier (e.g., logistic regression) is trained on the global class token $\mathbf{z}_{\text{cls}}^L$ to predict the biomarker label:

$$\hat{y} = \sigma(\mathbf{W}_{\text{lp}} \mathbf{z}_{\text{cls}}^L + b), \quad (4)$$

where \mathbf{W}_{lp} and b are trainable parameters, and $\sigma(\cdot)$ denotes the sigmoid or softmax activation depending on the task. While efficient, this approach relies solely on the global representation $\mathbf{z}_{\text{cls}}^L$ and thus fails to leverage the rich local cues and spatial information encoded in the patch tokens $\{\mathbf{z}_i^L\}_{i=1}^N$, such as cell morphology and intra-tissue relations.

2.2.3 Attention Pooling.

To overcome this limitation and capture hierarchical information across both global and local levels, we introduce an **attention pooling** mechanism that aggregates patch-level and cell-level embeddings guided by the class token. Specifically, the final representation \mathbf{h} is computed as:

$$\mathbf{h} = \text{Attn}(\mathbf{Q} = \mathbf{z}_{\text{cls}}^L, \mathbf{K} = \mathbf{Z}_{\text{patch}}^L, \mathbf{V} = \mathbf{Z}_{\text{patch}}^L), \quad (5)$$

The aggregated feature \mathbf{h} combines global and fine-grained local information, which is subsequently fed into a classification head:

$$\hat{y} = \sigma(\mathbf{W}_{\text{attn}} \mathbf{h} + b). \quad (6)$$

This hierarchical attention pooling enables the model to retain cell-level morphological details while preserving the global tissue context, leading to more accurate and interpretable biomarker predictions, which will be evaluated in the following section.

3 Results

3.1 Extensive Multi-Center Multi-Tasks Evaluation

We validate our method with five diverse classification tasks across four centers and three tumour types:

3.1.1 Colorectal Cancer (CRC) Tissue Detection

To evaluate our method on colorectal cancer (CRC) tissue, we used two public histopathology datasets: **NCT-CRC-HE-100K** and **NCT-CRC-HE-100K-NONORM** [27]. Both contain non-overlapping 224×224 px image patches at $0.5 \mu\text{m}$ per pixel, extracted from hematoxylin & eosin (H&E) stained slides of human colorectal adenocarcinoma.

The **CRC-Norm** task is based on the color-normalized dataset **NCT-CRC-HE-100K**, which includes 100,000 image patches from 86 slides across nine tissue classes. Color normalization was performed using Macenko’s method [28]. The validation set **CRC-VAL-HE-7K** contains 7,180 patches from 50 independent patients with no patient overlap.

The **CRC-Unnorm** task uses the non-normalized version **NCT-CRC-HE-100K-NONORM**, created from the same raw data but without color standardization, thereby preserving natural stain variability. This setup allows evaluation of model robustness under realistic staining differences. All tissue samples were collected at the National Center for Tumor Diseases (NCT, Heidelberg) and the University Medical Center Mannheim (UMM).

3.1.2 Colorectal Polyps Patterns Detection.

To further evaluate generalization, we used the **MHIST** dataset [29], which contains 3,152 H&E stained FFPE image patches (224×224 px) of colorectal polyps collected at Dartmouth-Hitchcock Medical Center (DHMC). All images were de-identified and annotated by seven board-certified pathologists for the predominant histological pattern. The **MHIST** task follows the default binary classification setup distinguishing *Hyperplastic Polyps (HP)* from *Sessile Serrated Adenomas (SSA)*, a clinically important yet challenging distinction due to high inter-pathologist variability. HPs are typically benign, whereas SSAs are precancerous lesions requiring earlier clinical follow-up.

3.1.3 Breast Cancer Detection.

We further included the **BACH** dataset [30], which consists of H&E stained breast histology microscopy images for breast cancer classification. The dataset contains 400 RGB images (2048×1536 px, $0.42 \mu\text{m}/\text{pixel}$), evenly distributed across four diagnostic categories: *Normal*, *Benign*, *In situ carcinoma*, and *Invasive carcinoma*. Each image was labeled according to the predominant tissue type by two expert pathologists, with any disagreements excluded from the final set. We followed the standard image-level classification setup provided in the challenge, using the official train–test split and evaluation protocol.

3.1.4 Clear Cell Renal Cell Carcinoma Detection.

We additionally evaluated our approach on the **CCRCC** dataset [31], derived from H&E slides of clear cell renal cell carcinoma (CCRCC) from the Cancer Genome Atlas (TCGA) and the Helsinki cohorts. The **tissue classification** task includes 52,713

image tiles (300×300 px) covering six tissue textures: *Cancer*, *Normal*, *Stroma*, *Blood*, *Empty*, and *Other*. Tiles were randomly extracted from TCGA-KIRC and Helsinki whole-slide images. We followed the default binary and multi-class setups provided with the dataset to assess tissue classification and immune infiltration prediction.

3.2 Quantitative Comparison to SOTA methods

3.2.1 Comparison Models

We exhaustively compare our method with the following several REAL SOTA FM methods:

(1) **DinoV2-L** [20], published by Meta AI, marked a new milestone in the era of vision foundation models. It was pretrained on 142 million natural images and distilled from a larger teacher model, demonstrating strong generalization across diverse visual tasks. (2) **DinoV3-L** [23], also developed by Meta, builds upon DINOv2 by scaling both data and architecture. It is pretrained on 1.7 billion images, introduces more flexible positional embeddings, and employs a novel post-training regularization strategy to enhance patch-token perceptual representation. (3) **UNI** [7], proposed by Harvard Medical School (Mahmood Lab), adapts the DINOv2 self-supervised pretraining framework to digital pathology. It was further fine-tuned with over 100 million patches derived from 100,000 private H&E whole-slide images (WSIs), forming one of the first large-scale pathology foundation models. (4) **UNI2**, extends UNI with larger model capacity and expanded data coverage, incorporating over 200 million histopathology patches from more than 350,000 WSIs. (5) **Virchow2** [8], introduced by Paige in collaboration with Microsoft, represents another major step forward in computational pathology foundation models. It integrates pathology-specific data augmentations, multi-magnification training, and stronger regularization, and was trained on over 3.5 million WSIs using a ViT-H/14 architecture with more than 600 million parameters. (6) **Conch** [32] leverages over 1.17 million image-caption pairs collected from diverse histopathology datasets and biomedical literature, integrating both visual and textual modalities through task-agnostic contrastive pretraining. (7) **Conch 1.5**, extends the CONCH framework with expanded datasets (over 4M image-caption pairs) and bigger patch-size. Its bigger embedding size improves multi-modal representation ability.

3.2.2 Measuring Patch-level classification performances

We report the performance of all evaluated methods under diverse classification tasks (see Fig. 2). In most of the classification tasks, our method consistently outperforms others except for MHIST dataset, where UNI achieves the best result. Our model surpasses the next-best method by **8.3% BACC in the most favorable case**, with an average improvement of **1.2% across all tasks**.

3.3 Ablation study of pretraining and validation choices

We summarize the impact of different pre-training and inference strategies, including staining augmentation and attention-pooling in the Table 1.

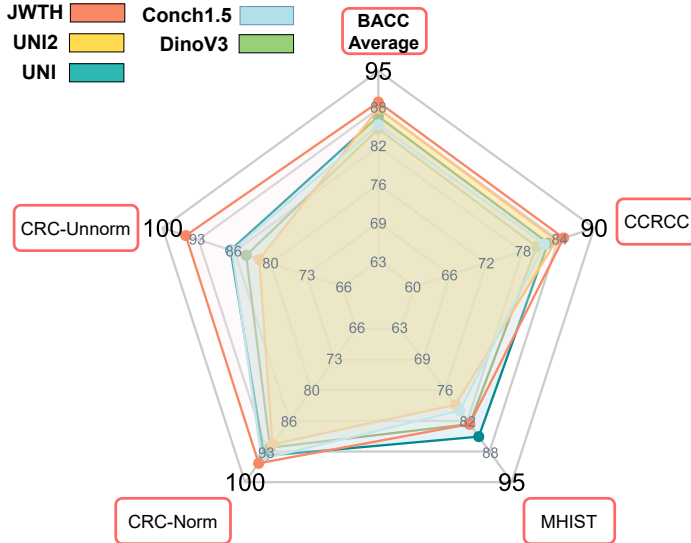


Fig. 2 Performances of different models on patch-level classification tasks. Balanced accuracy (BACC) is taken as the performance metric.

Table 1 Ablation study for model and training designs.

Default DINOv3	Staining Augmentation	Linear Probing	Atten Pooling	Balanced Acc Average
✓		✓		81.3
✓	✓	✓		83.6 (2.3 \uparrow) ¹
✓	✓		✓	86.9 (3.3 \uparrow) ²

¹Performance gain achieved by adding staining augmentation.

²Performance gain achieved by replacing linear probing with attention pooling.

4 Conclusion

In this work, we presented JWTH, a pathology foundation model that advances AI-based biomarker detection beyond traditional linear probing. By introducing a **Joint-Window Token Hierarchy**, JWTH effectively bridges global and cellular representations, enabling the model to capture fine-grained morphological cues while preserving contextual tissue structure. Through large-scale pretraining and cell-centric post-tuning, JWTH achieves both interpretability and robustness across diverse staining conditions and institutions. Comprehensive evaluations across six tasks, four biomarkers, and eight independent cohorts demonstrate that JWTH consistently surpasses state-of-the-art pathology foundation models in accuracy and generalization. These results underscore the potential of hierarchical token-based architectures to

serve as reliable AI biomarkers, offering a scalable path toward clinically actionable digital pathology.

References

- [1] Tan-Garcia, A., Chua, T.H., Leow, W.-Q.: Computational pathology in the age of artificial intelligence—embrace not fear. *The Journal of Pathology: Clinical Research* **11**(5), 70049 (2025)
- [2] Campanella, G., Kumar, N., Nanda, S., Singi, S., Fluder, E., Kwan, R., Muehlstedt, S., Pfarr, N., Schüffler, P.J., Häggström, I., et al.: Real-world deployment of a fine-tuned pathology foundation model for lung cancer biomarker detection. *Nature Medicine*, 1–9 (2025)
- [3] Matthews, G.A., McGenity, C., Bansal, D., Treanor, D.: Public evidence on ai products for digital pathology. *NPJ Digital Medicine* **7**(1), 300 (2024)
- [4] Kazemi, A., Rasouli-Saravani, A., Gharib, M., Albuquerque, T., Eslami, S., Schüffler, P.J.: A systematic review of machine learning-based tumor-infiltrating lymphocytes analysis in colorectal cancer: Overview of techniques, performance metrics, and clinical outcomes. *Computers in Biology and Medicine* **173**, 108306 (2024)
- [5] McGenity, C., Clarke, E.L., Jennings, C., Matthews, G., Cartlidge, C., Stocken, D.D., Treanor, D.: Artificial intelligence in digital pathology: a systematic review and meta-analysis of diagnostic test accuracy. *NPJ digital medicine* **7**(1), 114 (2024)
- [6] Dippel, J., Feulner, B., Winterhoff, T., Milbich, T., Tietz, S., Schallenberg, S., Dernbach, G., Kunft, A., Heinke, S., Eich, M.-L., et al.: Rudolfv: a foundation model by pathologists for pathologists. *arXiv preprint arXiv:2401.04079* (2024)
- [7] Chen, R.J., Ding, T., Lu, M.Y., Williamson, D.F., Jaume, G., Song, A.H., Chen, B., Zhang, A., Shao, D., Shaban, M., et al.: Towards a general-purpose foundation model for computational pathology. *Nature medicine* **30**(3), 850–862 (2024)
- [8] Zimmermann, E., Vorontsov, E., Viret, J., Casson, A., Zelechowski, M., Shaikovski, G., Tenenholtz, N., Hall, J., Klimstra, D., Yousfi, R., et al.: Virchow2: Scaling self-supervised mixed magnification models in pathology. *arXiv preprint arXiv:2408.00738* (2024)
- [9] Wang, X., Zhao, J., Marostica, E., Yuan, W., Jin, J., Zhang, J., Li, R., Tang, H., Wang, K., Li, Y., et al.: A pathology foundation model for cancer diagnosis and prognosis prediction. *Nature* **634**(8035), 970–978 (2024)
- [10] Liu, J., Deng, X., Li, H., Kazemi, A., Grashei, C., Wilkens, G., You, X., Groll, T., Navab, N., Mogler, C., et al.: From pixels to pathology: Restoration diffusion

for diagnostic-consistent virtual ihc. arXiv preprint arXiv:2508.02528 (2025)

- [11] Wu, K., Jiang, Z., Tang, K., Shi, J., Xie, F., Wang, W., Wu, H., Zheng, Y.: Pan-cancer histopathology wsi pre-training with position-aware masked autoencoder. *IEEE Transactions on Medical Imaging* (2024)
- [12] Farahmand, S., Fernandez, A., Ahmed, F., Rimm, D., Chuang, J., Reisenbichler, E., Zarringhalam, K.: Her2 and trastuzumab treatment response h&e slides with tumor roi annotations. *The Cancer Imaging Archive* (2022)
- [13] Li, D., Wan, G., Wu, X., Wu, X., Nirmal, A.J., Lian, C.G., Sorger, P.K., Semenov, Y.R., Zhao, C.: A survey on computational pathology foundation models: Datasets, adaptation strategies, and evaluation tasks. arXiv preprint arXiv:2501.15724 (2025)
- [14] Couture, H.D., Williams, L.A., Geradts, J., Nyante, S.J., Butler, E.N., Marron, J., Perou, C.M., Troester, M.A., Niethammer, M.: Image analysis with deep learning to predict breast cancer grade, er status, histologic subtype, and intrinsic subtype. *NPJ breast cancer* **4**(1), 30 (2018)
- [15] Chen, R.J., Lu, M.Y., Wang, J., Williamson, D.F., Rodig, S.J., Lindeman, N.I., Mahmood, F.: Pathomic fusion: an integrated framework for fusing histopathology and genomic features for cancer diagnosis and prognosis. *IEEE Transactions on Medical Imaging* **41**(4), 757–770 (2020)
- [16] Xu, Z., Du, X., Kang, Y., Lv, H., Li, M., Yang, W., Cui, L., Li, H., Xing, Y., Feng, J., *et al.*: Addressing sparse annotation: a novel semantic energy loss for tumor cell detection from histopathologic images. In: *2023 IEEE International Conference on Bioinformatics and Biomedicine (BIBM)*, pp. 1588–1595 (2023). IEEE
- [17] Liu, J., Li, H., Yang, C., Deutges, M., Sadafi, A., You, X., Breininger, K., Navab, N., Schüffler, P.J.: Hasd: Hierarchical adaption for pathology slide-level domain-shift. In: *International Conference on Medical Image Computing and Computer-Assisted Intervention*, pp. 332–342 (2025). Springer
- [18] Pati, P., Jaume, G., Foncubierta-Rodriguez, A., Feroce, F., Anniciello, A.M., Scognamiglio, G., Brancati, N., Fiche, M., Dubruc, E., Riccio, D., *et al.*: Hierarchical graph representations in digital pathology. *Medical image analysis* **75**, 102264 (2022)
- [19] Huang, Y., Huang, Z., Xiang, L., Yang, Q., Yin, H.: Pathohr: Hierarchical reasoning for vision-language models in pathology. arXiv preprint arXiv:2509.06105 (2025)
- [20] Oquab, M., Darcet, T., Moutakanni, T., Vo, H., Szafraniec, M., Khalidov, V., Fernandez, P., Haziza, D., Massa, F., El-Nouby, A., *et al.*: Dinov2: Learning robust

- visual features without supervision. arXiv preprint arXiv:2304.07193 (2023)
- [21] He, K., Chen, X., Xie, S., Li, Y., Dollár, P., Girshick, R.: Masked autoencoders are scalable vision learners. In: Proceedings of the IEEE/CVF Conference on Computer Vision and Pattern Recognition, pp. 16000–16009 (2022)
- [22] Shen, Y., Luo, Y., Shen, D., Ke, J.: Randstainna: Learning stain-agnostic features from histology slides by bridging stain augmentation and normalization. In: International Conference on Medical Image Computing and Computer-Assisted Intervention, pp. 212–221 (2022). Springer
- [23] Siméoni, O., Vo, H.V., Seitzer, M., Baldassarre, F., Oquab, M.: Dinov3. arXiv preprint arXiv:2508.10104 **3**(4) (2025)
- [24] Jing, L., Vincent, P., LeCun, Y., Tian, Y.: Understanding dimensional collapse in contrastive self-supervised learning. arXiv preprint arXiv:2110.09348 (2021)
- [25] Fan, D., Tong, S., Zhu, J., Sinha, K., Liu, Z., Chen, X., Rabbat, M., Ballas, N., LeCun, Y., Bar, A., et al.: Scaling language-free visual representation learning. arXiv preprint arXiv:2504.01017 (2025)
- [26] Steiner, A., Kolesnikov, A., Zhai, X., Wightman, R., Uszkoreit, J., Beyer, L.: How to train your vit? data, augmentation, and regularization in vision transformers. arXiv preprint arXiv:2106.10270 (2021)
- [27] Kather, J.N., Halama, N., Marx, A.: 100,000 histological images of human colorectal cancer and healthy tissue, april 2018. URL <https://doi.org/10.5281/zenodo.1214456> (2024)
- [28] Macenko, M., Niethammer, M., Marron, J.S., Borland, D., Woosley, J.T., Guan, X., Schmitt, C., Thomas, N.E.: A method for normalizing histology slides for quantitative analysis. In: 2009 IEEE International Symposium on Biomedical Imaging: from Nano to Macro, pp. 1107–1110 (2009). IEEE
- [29] Wei, J., Suriawinata, A., Ren, B., Liu, X., Lisovsky, M., Vaickus, L., Brown, C., Baker, M., Tomita, N., Torresani, L., et al.: A petri dish for histopathology image analysis. In: International Conference on Artificial Intelligence in Medicine, pp. 11–24 (2021). Springer
- [30] Araújo, T., Aresta, G., Castro, E., Rouco, J., Aguiar, P., Eloy, C., Polónia, A., Campilho, A.: Classification of breast cancer histology images using convolutional neural networks. PloS one **12**(6), 0177544 (2017)
- [31] Brummer, O., Pölönen, P., Mustjoki, S., Brück, O.: Computational textural mapping harmonises sampling variation and reveals multidimensional histopathological fingerprints. British Journal of Cancer **129**(4), 683–695 (2023)

- [32] Lu, M.Y., Chen, B., Williamson, D.F., Chen, R.J., Liang, I., Ding, T., Jaume, G., Odintsov, I., Le, L.P., Gerber, G., *et al.*: A visual-language foundation model for computational pathology. *Nature medicine* **30**(3), 863–874 (2024)